Published in final edited form as:

Adv Energy Mater. 2017 September 6; 7(17): . doi:10.1002/aenm.201700358.

Ultrathin Graphene–Protein Supercapacitors for Miniaturized Bioelectronics

Islam M. Mosa,
Department of Chemistry, University of Connecticut, Storrs, CT 06269, USA

Department of Chemistry, Tanta University, Tanta 31527, Egypt

Dr. Ajith Pattammattel,
Department of Chemistry, University of Connecticut, Storrs, CT 06269, USA

Karteek Kadimisetty,
Department of Chemistry, University of Connecticut, Storrs, CT 06269, USA

Dr. Paritosh Pande,
Department of Chemistry, University of Connecticut, Storrs, CT 06269, USA

Dr. Maher F. El-Kady,
Department of Chemistry and Biochemistry and California, NanoSystems Institute, University of California, Los Angeles (UCLA), Los Angeles, CA 90095, USA

Department of Chemistry, Faculty of Science, Cairo University, Giza 12613, Egypt

Gregory W. Bishop [Prof.],
Department of Chemistry, University of Connecticut, Storrs, CT 06269, USA

Department of Chemistry, East Tennessee State, Johnson City 37614, USA

Marc Novak,
Department of Molecular and Cell Biology, University of Connecticut, Storrs, CT 06269, USA

Richard B. Kaner [Prof.],
Department of Chemistry and Biochemistry and California, NanoSystems Institute, University of California, Los Angeles (UCLA), Los Angeles, CA 90095, USA

Department of Materials Science and Engineering, UCLA, Los Angeles, CA 90095, USA

Ashis K. Basu [Prof.],
Department of Chemistry, University of Connecticut, Storrs, CT 06269, USA

Challa V. Kumar [Prof.], and
Department of Chemistry, University of Connecticut, Storrs, CT 06269, USA

Department of Molecular and Cell Biology, University of Connecticut, Storrs, CT 06269, USA

Correspondence to: Islam M. Mosa; Challa V. Kumar; James F. Rusling.

Supporting Information
Supporting Information is available from the Wiley Online Library or from the author.

Institute of Materials Science, University of Connecticut, 97 North Eagleville Road, Storrs, CT 06269, USA

James F. Rusling [Prof.]
Department of Chemistry, University of Connecticut, Storrs, CT 06269, USA

Institute of Materials Science, University of Connecticut, 97 North Eagleville Road, Storrs, CT 06269, USA

Department of Surgery and Neag Cancer, Center University of Connecticut Health Center, Farmington, CT 06032, USA

School of Chemistry, National University of Ireland, Galway, University Road, Galway, Ireland

Abstract

Nearly all implantable bioelectronics are powered by bulky batteries which limit device miniaturization and lifespan. Moreover, batteries contain toxic materials and electrolytes that can be dangerous if leakage occurs. Herein, an approach to fabricate implantable protein-based bioelectrochemical capacitors (bECs) employing new nanocomposite heterostructures in which 2D reduced graphene oxide sheets are interlayered with chemically modified mammalian proteins, while utilizing biological fluids as electrolytes is described. This protein-modified reduced graphene oxide nanocomposite material shows no toxicity to mouse embryo fibroblasts and COS-7 cell cultures at a high concentration of 1600 μg mL^{-1} which is 160 times higher than those used in bECs, unlike the unmodified graphene oxide which caused toxic cell damage even at low doses of 10 μg mL^{-1}. The bEC devices are 1 μm thick, fully flexible, and have high energy density comparable to that of lithium thin film batteries. COS-7 cell culture is not affected by long-term exposure to encapsulated bECs over 4 d of continuous charge/discharge cycles. These bECs are unique, protein-based devices, use serum as electrolyte, and have the potential to power a new generation of long-life, miniaturized implantable devices.

Keywords

bioelectrochemical capacitors; biosupercapacitor-energy harvester; graphene-proteins; implantable supercapacitors; toxicity

1. Introduction

Implantable medical devices have revolutionized treatment of some chronic diseases. For example, modern cardiac pacemakers can monitor and control the patient's heart function, and report critical events to hospital control centers. However, powering such implanted devices by batteries creates problems,[1] because these devices must be replaced when the battery is drained. This necessitates that the patient undergo painful surgery at significant expense. Therefore, a few researchers are exploring battery-free implantable devices by harvesting energy directly from the human body,[2] for example, from motion, body heat, hydraulic energy of the circulatory system, or even from glucose in body fluids.[3] Energy harvesters can convert this ambient energy into electricity that is sufficient to power many implantable medical devices.[2a,4] Unlike batteries, human-powered energy harvesters could

power existing implants indefinitely. Recently, researchers have successfully developed an implantable nanogenerator in a living rat that works by extracting energy from its periodic breathing. This energy was used to power a prototype pacemaker.[5] In another example, a mass imbalance oscillation generator taken from a commercially available automatic wrist watch was used to harvest the kinetic energy from the beating heart of a living sheep and the generated power (16.7 μW) was sufficient to provide 1 μW of power[6] to run a pacemaker.

Biofriendly, protein-based batteries or supercapacitors that use human body fluids (serum/urine) as electrolytes and are harmless to biological systems during their functional performance are highly promising but currently do not exist. As a first step toward such devices, we demonstrate here a revolutionary, protein-based supercapacitor, which uses benign electrolytes and electrode materials that are nontoxic to living cells.

Supercapacitors are high-performance electrochemical capacitors (ECs) that store energy at much higher power density than batteries. Power systems for implantable devices as described above require an intermediate energy storage system such as ECs for their operation.[7] Basically, by storing the generated energy in an EC, the output power can periodically drive existing medical implants.[5] However, like other implanted medical devices there are some stringent requirements for this EC. First, it must be safe during operation, and have predictable performance and high reliability.[8] Second, this EC should provide service over many years with no maintenance required. It is also important to have high volumetric energy density to enable the miniaturization of the entire implanted system (Figure 1).

Compared to batteries, ECs have faster charge–discharge rates, lower internal resistance, higher power density, better cycling stability, and the ability to use external fluids as electrolytes.[9] These devices have the potential to power a new generation of implantable devices such as cardiac and gastric pacemakers, deep brain, bladder, and bone stimulators, automated drug delivery systems, artificial vision, and biosensors.[10] However, ECs are currently limited by relatively low volumetric and gravimetric capacitances, and low energy densities (energy stored per unit volume or mass) that are less than those of batteries.[11] In addition, batteries in general are considered the least “green” component in any electronic device.[12] They often use toxic materials and operate on liquid electrolytes, which can be very harmful if leakage occurs. Using such batteries for implantable medical devices not only make them bulky but also raises safety concerns. Thus, rationally designing green and sustainable bioelectrochemical capacitors (bECs)[13], also called biosupercapacitor, with high volumetric energy density is highly desirable. It is also crucial that these bECs use electrode materials and electrolytes that are safe to living cells.

Graphene sheets feature single layers of carbon atoms with unique electrical properties that are promising for designing ultrathin bECs and other novel technological applications.[14] It is an attractive nanomaterial for implantable bECs, given its high theoretical capacitance of ≈550 F g^{-1} and its rich surface chemistry which enables further processing into composite materials with desirable properties.[15] Graphene has attracted great attention for the design of ultrathin ECs. By attaching cation-derivatized (cationized) bovine serum albumin (cBSA) to the surface of graphene oxide (GO) as a nanospacer and further deposition of heme

protein myoglobin in a layer-by-layer (LbL) process, followed by electrochemical reduction, we have developed graphene-based bECs with an ultrahigh volumetric capacitance in biofluids up to 655 F cm^{-3} at a scan rate of 100 mV s^{-1}, and 534 F cm^{-3} at a current density of 2.5 A g^{-1}. Energy density reaches up to 1.8 mWh cm^{-3}, which is 3–11 times higher than commercially available thin-film ECs. They are thinner (1.14 μm) than a human hair and can provide high power density. Unlike pristine graphene which poses potential risks to human cells,[16] the new hybrid material showed no signs of cell toxicity at concentrations 160 times higher than those used in our bECs, and the encapsulated device showed no adverse effects on cells after 4 d of continuous charge/discharge cycles. This paper presents a new platform for the design of ultrathin bECs utilizing for the first time human biofluids as electrolytes for the development of the next-generation implantable medical devices (Figure 1).

2. Results and Discussion

To fully realize the potential of graphene for implantable capaci tive energy storage, we designed a bottom up approach for the assembly of ultrathin graphene-protein-based electrodes (Figure 2). We fabricated these bECs using novel biophilized graphene oxide (bGO) nanocomposite that we developed featuring GO sheets modified with cBSA. The latter material is BSA with chemically attached protonated amine groups to enhance positive charge and proton transfer capacity.[17] We then used LbL deposition[18] to fabricate electrodes of alternate layers of bGO and myoglobin (Mb) onto a 1.0 cm^2 ultrathin gold sheet to form several graphene oxide modified proteins (bGO/Mb) bilayers (note: one bilayer refers to one bGO layer). Then bGO/Mb was electrochemically reduced to brGO/Mb (brGO = biophilized reduced graphene oxide) (Figure 2g). A film of three layers of brGO sandwiching two layers of Mb gave the largest capacitance per unit volume, up to 534 F cm^{-3} in human urine at 2.5 A g^{-1} (contribution of current collector and separator is subtracted, see the Supporting Information for details). bEC devices made from these electrodes were able to utilize cell culture media, and mammalian biofluids as electrolytes for high capacitance output with no measurable signs of cytotoxicity in cell culture media.

In this design, cBSA and Mb should render graphene more compatible with living cells, and provide a good source of heteroatoms to improve the specific capacitance of graphene by introducing pseudocapacitive behavior.[19] These proteins have a good adsorption character and their charge can be easily controlled by changing the pH which make them an excellent candidate for electrode fabrication. Moreover, proteins act as polyionic nanospacers to prevent the restacking of graphene that often limits the access of the ions to the sheets and undermines its electrochemical performance. A gold current collector was employed in the cell design, since gold is among the safest materials for medical applications.[20] Other designs have been reported using reduced graphene oxide assembled with polymers that achieved good capacitive performance, but using toxic polymers as part of their electrode materials as well as using toxic electrolytes saturated separators limit their use for implantable biomedical applications.[15b]

In order to understand the capacitive behavior of these graphene–protein bECs, different protein films were LbL assembled with brGO (three brGO layers sandwiching two protein

layers) and their electrochemical performance was evaluated using charge/discharge curves and cyclic voltammetry (CV) (Table S1, Figure S1 and S2, Supporting Information). Utilizing calf serum as electrolyte at a current density of 0.005 mA cm^{-2}, Mb showed the highest areal capacitance reaching 1526 μF cm^{-2}, followed by cytochrome-C (Cyt-C) with a capacitance of 1175 μF cm^{-2}, then hemoglobin (Hb), glucose oxidase (GOx), and finally catalase (Cat) in order of decreasing the areal capacitance (Figure S1, Table S1, Supporting Information). Proteins are rechargeable by protonation/deprotonation through their charged residues, that is, charged amino acid side chains (lysine, arginine, histidine, glutamic acid, and aspartic acid).[21] Protonation/deprotonation can be used by organic compounds to store the capacitive charge, which has been demonstrated for their use in ultrafast supercapacitors.[22] By calculating the total number of charged amino acid residues (protonatable sites) in each protein and normalizing them to the molar mass of the protein, a strong correlation with the areal capacitance was discovered (Figure 3i; Table S1, Supporting Information). Myoglobin had the highest ratio of charged residue/molar mass (Z/M) and the highest areal capacitance, followed by Cyt-C, Hb, and GOx in order of decreasing both the Z/M ratio and the areal capacitance (Figure 3i; Table S1, Supporting Information). Catalase showed moderate Z/M ratio but exhibited low areal capacitance due to its large molecular size and highly negative hydropathy index (Figure 3i; Table S1, Supporting Information). This suggests a key role of the number of protonatable sites in the capacitive performance of the graphene–protein films. Based on these results, Mb nano-composite with brGO was chosen and further explored for the development of bECs.

Characterization of the brGO/Mb electrode using scanning electron microscopy (SEM) revealed that brGO/Mb films adsorbed to the striated gold current collectors were continuous and relatively uniform (Figure S3, Supporting Information). Tapping mode atomic force microscopy (AFM) images showed a uniform first layer of poly(diallyldimethyl ammonium) chloride (PDDA) (Figure 3a). The adsorption of bGO results in a continuous layer of overlapping GO sheets with small islands of cBSA as shown in Figure 3b. The incorporation of the Mb layer increases the film roughness due to its globular nature (Figure 3c). Addition of another layer of bGO on this surface results in a sheet-like covering on the Mb layer (Figure 3d). Overall, AFM images reveal the homogeneous coating of the LbL film on the gold current collector.

We used quartz crystal microbalance (QCM) to monitor and control the LbL assembly of the electrode material. We observe from Figure 3e that the bGO/Mb film grows almost linearly as a function of the number of layers. The electrochemical reduction of this bGO/Mb film is associated with a decrease in the electrode mass and thickness, suggesting the successful removal of residual oxygen functionalities from the surface of the graphene oxide.[23] QCM estimates a nominal thickness of 32 ± 2 nm for the brGO/Mb active film (Figure 3e; see the Supporting Information for more details), while SEM cross section imaging after cutting with a focused ion beam gave 26 ± 5 nm for the same film (Figure S4, Supporting Information). Thus, the average thickness of brGO/Mb/brGO/Mb/brGO from the SEM and QCM was 29 ± 4 nm. Analysis of the films by Raman spectroscopy showed an increase in the ratio of the D band to the G band (I_D/I_G) for brGO (1.1) compared to bGO (0.94) (Figure 3f), suggesting that the reduction resulted in structural modification of graphene oxide sheets

with the introduction of defects. Moreover, the 2D and S3 bands showed notable increases after reduction suggesting the better graphitization in brGO.[24]

The unique spacing achieved by Mb spreading on the bGO reduced the extent of **π**–**π** stacking between adjacent layers and separated them more efficiently (Figures S5–S7, Supporting Information). This was confirmed by the shift of the characteristic GO X-ray powder diffraction (XRD) peak in the bGO/Mb film to a lower diffraction angle as compared to the as-prepared GO indicating the increase of the intersheet distance due to Mb spacing (Figure S6, Supporting Information). In addition, Raman spectra of different proteins bound directly to GO were compared to the Raman spectrum of the GO-only sample. Results show that the Mb–GO film has a sharp, relatively high intensity 2D peak compared to other proteins bound GO or the as-prepared GO sample indicating fewer layers of GO sheets and hence better spacing in case of GO/Mb films (Figure S7, Supporting Information). This may be attributed to the small size and the higher electrostatic attraction of Mb to GO because of Mb's higher Z/M ratio (Figure 3i; Table S1, Supporting Information).

Binding of Mb to bGO was quantified and the bound protein structure examined by circular dichroism (CD) spectroscopy (Figure 3g,h). CD spectra indicated a loss of secondary structure of the bound Mb. Other proteins were also tested as alternatives to Mb, most of these retained their secondary structures on binding to bGO,[17] but capacitive performance was the best with Mb (Figure 3i). Proteins in the film increased the capacitance per unit area, up to five times when compared to the capacitances of the corresponding films made from drop-casted reduced graphene oxide, which lacked the proper spacing of sheets and the pseudocapacitance of the heteroatom-rich interlayers (Figure S8, Supporting Information) with charged residues and protonatable sites which are required for charge storage by protonation/deprotonation as the brGO layers are charged up. In addition, brGO interlayered with Mb (brGO/Mb) showed ≈2 times higher capacitance versus brGO-only films drop-cast on the electrodes (Figure S9, Supporting Information), indicating the important capacitive role of Mb in brGO/Mb films.

The electrochemical reduction of the film was achieved in 10×10^{-3} M acetate buffer, pH 5.5 containing 0.5 M potassium bromide (KBr) at constant potential −1.2 V versus saturated calomel electrode (SCE) for 70 s. The reduction of bGO in the film to brGO was indicated by the change of film color from brown to black, and is supported by a reduction peak for bGO found at −0.95 V versus SCE by CV that disappears upon subsequent scans (Figure S10a, Supporting Information). In addition, a dramatic increase in capacitance was found after bGO reduction to brGO (Figure 4a; Figure S10b,c, Supporting Information). CV profiles showed characteristic Fe^{III}/Fe^{II} peaks of Mb at −0.3 V versus SCE in acetate buffer. These characteristic peaks appeared before and after reducing the film for 3 s, but continued reduction for 70 s caused a large increase in the charging current and loss of the Mb peaks (Figure S10, Supporting Information).

The iron heme center of hemoproteins is an important active center for a number of catalytic reactions,[25] and was also reported to contribute to capacitance of thick proteins films supported on nickel foam electrodes.[26] However, loss of the characteristic redox peaks of

the Fe^{III}/Fe^{II} of the heme center after electrochemical reduction (Figure S10, Supporting Information), along with the loss of the protein secondary structure as revealed by CD (Figure 3h), confirm that Mb is denatured in the brGO/Mb electrodes and the heme center is lost or deactivated, which suggests a minor role of the Fe^{III}/Fe^{II} heme redox couple in the capacitive behavior of the brGO/Mb electrodes.

Myoglobin has the highest Z/M ratio among the studied proteins, and yet Mb-only films had low specific capacitance of 16.6 F g^{-1} (Figure S11, Supporting Information). The low capacitance of Mb in the absence of graphene is due to the poor electrical conductivity of Mb-only films. The electrical conductivity of the Mb alone and in the LbL assembled film with brGO were measured using the 4 probe technique. Mb showed low electrical conductivity of 3.6×10^{-8} S cm^{-1} at room temperature due to its insulating nature which explains the poor electron flow through thick Mb films and its low specific capacitance. However, the introduction of brGO to the Mb films increased the electrical conductivity by about five orders of magnitude reaching 0.003 S cm^{-1} at room temperature. The electrical conductivity of the brGO/Mb electrode was further explored at different temperatures using a two-electrode setup (Figure S12, Supporting Information). The brGO/Mb electrode showed good thermal stability and increase in conductivity as the brGO/Mb electrode was heated up to 150 °C, suggesting that the brGO/Mb electrodes are thermally stable at temperatures far beyond those needed for implantable applications.

The electrochemical performance of the brGO/Mb electrodes was further studied to assess capacitive efficiency as implantable bECs. The capacitive behavior depends strongly on the number of bilayers. The areal capacitance increased almost linearly up to three bilayers, after which a plateau is observed (Figure 4b; Figure S13, Supporting Information). This is likely due to the low conductivity of the Mb layers that limit electron transport between the top layer and the current collector for thicker films. The capacitance functionality of each of the five layers of the brGO/Mb film and the supports were evaluated in calf serum using charge/discharge curves at 0.005 mA cm^{-2} (Figures S14 and S15, Table S2, Supporting Information). The areal capacitance of the positively charged gold current collector (with PDDA adsorbed on the surface) is 90 μF cm^{-2} which represents ≈6% of the areal capacitance of the final brGO/Mb electrode. The capacitance of the current collector was subtracted from the capacitance of all other samples. The adsorption of the first bGO layer followed by electrochemical reduction to brGO resulted in a 2.0 μg cm^{-2} brGO layer as measured by QCM with an areal capacitance of 462 μF cm^{-2} and a gravimetric capacitance of 232 F g^{-1}. The first brGO layer represents 40% of the mass of the final brGO/Mb film and 30.3% of its areal capacitance. The adsorption of the positively charged Mb as a second layer resulted in a significant increase in the areal capacitance reaching 847 μF cm^{-2} and increasing the gravimetric capacitance of the assembled film to 260 F g^{-1} indicating the key role of myoglobin in enhancing the capacitive performance of the device. The areal capacitance increased by adding more brGO and Mb layers achieving the maximum areal and gravimetric capacitance after five layers (brGO-Mb-brGO-Mb-brGO) with 1526 μF cm^{-2} and 306 F g^{-1}, respectively (Figure S14, Table S2, Supporting Information). A similar film was prepared by replacing the bGO with GO for the LbL assembly with Mb followed by electrochemical reduction to form rGO-Mb-rGO-Mb-rGO electrode abbreviated as (rGO/Mb) resulting in a gravimetric capacitance of 239 F g^{-1} which is 22% less than the

brGO/Mb electrode. The significant capacitance contribution of cBSA is due to its high charged amino acid content with 198 protonatable sites[27] per molecule scoring the second highest Z/M ratio (0.003) of the studied proteins after Mb. These results show the capacitive contribution of the proteins (cBSA and Mb) in enhancing overall capacitive behavior (Figure S14, Supporting Information). Based on these results, electrodes of three brGO layers alternated with two Mb layers achieved the maximum capacitance and were used for the subsequent device fabrication.

A photograph of a prototype implantable bEC is shown in Figure 4c. It was assembled from two brGO/Mb/brGO/Mb/brGO electrodes bound to a flexible thin gold foil with a thickness of 42 ± 8 nm (Figure S4, Supporting Information) obtained after etching away the plastic protective layer of a gold CD.[28] To get a neat and ultrathin EC, a layer of polyvinyl acetate gel saturated with electrolyte was loaded onto the electrodes to serve as both the separator and electrolyte with an average separator thickness of 992 nm (Figure S16, Supporting Information). This simplifies the processing of the electrodes into paper-like flexible bECs. The total thickness of the device is 1.14 μm, providing a thin, lightweight power source for implantable devices.

The packageless brGO/Mb bEC effectively utilized different biofluids in the surrounding medium as electrolytes including calf serum, cell culture media, and human urine. For comparison, we also tested the brGO/Mb bEC in 0.1 M sulfuric acid, a typical standard electrolyte (Figures S17 and S18, Supporting Information). It is important for ECs with high energy density to be characterized at high scan rates,[29] specially when used as a power source for implantable bioelectronics. This enables the fast charging of the current received from the nanogenerator and the fast discharging of the electrical signal to the implantable devices by the bEC. Therefore, we presented the bEC device capacitive performance at moderate-to-high current density and high scan rate ranges (Figure 4e; Figure S18, Supporting Information). Results show nearly rectangular CV shapes even at high scan rates of 1000 mV s^{-1}, indicating nearly ideal capacitive behavior (Figure 4d; Figure S19 and S20, Supporting Information). The maximum volumetric capacitance in biofluids (after subtracting the contribution of current collectors) was 655 F cm^{-3} at scan rate of 100 mV s^{-1} and 534 F cm^{-3} obtained at a current density of 2.5 A g^{-1} in human urine, while the volumetric capacitance in calf serum was 563 F cm^{-3} at 100 mV s^{-1} and 372 F cm^{-3} at 2.5 A g^{-1} (Figure 4e; Figure S18, Supporting Information). It is possible that the capacitance depends on the availability and type of ions present in these different electrolytes, illustrated by a 14% drop in capacitance when changing from human urine to calf serum (Figure S18, Supporting Information). The short-term cycling stability of the packageless bEC turns out to be excellent with only a 2% drop in capacitance after 5000 cycles in calf serum (Figure 4f). This good cycling performance in biofluids suggests the short-term stability of the packageless bECs operating in biological environment, while the long-term stability and toxicity of the device will be further tested when the device is dipped in living cell culture (Figure 5).

The excellent performance of brGO/Mb bECs was also confirmed from charge/discharge cycles (Figure 4g, and Figure S19 and S20, Supporting Information). Depending on the type of electrolyte, the brGO/Mb bEC can provide a high stack capacitance of ≈13–16 F cm^{-3}.

This was calculated based on the volume of the device stack, which includes the gold current collector, active materials, electrolyte, and separator. When compared with commercial electric double layer capacitors (EDLCs), the brGO/Mb can provide 25–400 times higher stack capacitance. Not only does the brGO/Mb device provide higher capacitance, but also exhibits excellent rate capability at high current densities up to 20 A cm^{-3} (Figure 4g). This remarkable performance can be attributed to the microstructure of the electrode featuring brGO/Mb layered films with different pore sizes due to the protein interlayers which may facilitate the ion movement during charge/discharge process (Figure S21, Supporting Information).[30]

In order to demonstrate the overall performance of the brGO/Mb bEC, we calculated its energy density and power density and the results are displayed in a Ragone plot (Figure S22, Supporting Information). The brGO/Mb bEC displays a high energy density of 1.1 W h kg^{-1} at a high power density of 116 W kg^{-1}, calculated based on the total mass of the device stack as illustrated in Figure S22 (Supporting Information). We have also produced the same plot using the volume of the device stack (Figure 4h). For comparison, we also tested the energy density and power density of a 300 μF/3 V aluminum electrolytic capacitor, 12 μA h/3.3 V Li thin film battery, 500 μA h/5 V Li thin film battery and three commercially available EDLCs designed for small-scale applications. The brGO/Mb bEC can provide a high energy density of 1.8 mW h cm^{-3}, which is comparable to Li thin film batteries and 3–11 times higher than thin film commercial EDLCs. The brGO/Mb device can also deliver about 100 times higher power density than Li thin film batteries which is sufficient to drive all implantable medical devices known to us (Figure 4h). It is worth mentioning here that the purpose of this work is to design ultrathin bECs for miniaturized implantable devices and therefore a comparison with conventional thick film electrodes seems irrelevant.

The brGO/Mb system described here is the first graphene–protein bEC, and shows superlative characteristics as a power source for implantable devices. For example, proteins have been used as a source for carbon electrodes by graphitization at 800 °C.[31] These devices do not feature intact proteins and have low capacitance. Redox hemin-based proteins were used to enhance pseudocapacitance on a nickel foam, but again low specific capacitances were obtained (e.g., hemoglobin 12 F g^{-1}) due to the low conductivity of the protein-only films.[26] In addition, supercapacitors fabricated from a biofilm of the conductive bacteria *Geobacter sulfurreducens* which is rich in cytochrome C protein was reported.[32] Using the live conductive bacterial biofilms as electrode material resulted in low specific capacitance, potential loss of conductivity after the bacteria die, and risks of infection if used in implantable biomedical devices. On the other hand, previous reports of DNA based ECs have been tested for their adverse effects on living cells, and showed mode rate-to-no toxicity signs on cells, but they had at best six times lower gravimetric capacitance than brGO/Mb bECs.[33]

Toward developing safe implantable bECs, toxicity and adverse effects of materials used to fabricate the bEC electrodes were studied using living mammalian cells. The toxicity of different concentrations of the as-prepared GO and bGO/Mb on COS-7 and mouse embryo fibroblast (MEF) cell lines was evaluated by optical microscopy and spectrophotometrically by employing WST-8 dye (water-soluble tetrazolium salt) as a chromogen. WST-8 is a

water-soluble, cell-permeable dye, which gets reduced by the active intracellular dehydrogenases (IDH) in the cell cytosol.[34] Quantitative reduction of WST-8 by IDH enables accurate quantification of the overall metabolic health of a living cell.

The native GO showed significant cell damage after being coincubated with COS-7 cells for 8 h at a 25 μg mL^{-1} dose resulting in 41% specific cell death as measured by trypan blue assay, significant cell shrinkage, and cell cycle arrest (Figure 5c; Table S3, Supporting Information), and ≈60% drop in IDH activity (Figure 5d). In contrast, no sign of cell toxicity was observed for bGO/Mb coincubated with COS-7 cells for 48 h at a dose as high as 1600 μg mL^{-1} with no statistically significant change in live/dead cell ratio (Figure 5b; Table S3, Supporting Information) or IDH activity compared to control cells (Figure 5e). These results suggest that native GO causes serious toxic effects and the metabolic health of live cells and should not be used directly in contact with human cells.[35] On the other hand, bGO/Mb was compatible with cells even at very high concentrations with little change in toxicity or metabolic health of cells at doses 160 times higher than those used in the bECs (Figure 5b,e; Table S3, Supporting Information). Results suggest that bGO/Mb is safe for living cells, and can be used for fabricating implantable packageless bECs working in open cell solution or encapsulated bECs.

Performance and toxicity of the packageless brGO/Mb bECs were evaluated in cell cultures of MEF and COS-7 cells in Dulbecco's modified Eagle medium (DMEM) while these bECs were subject to continuous cycling test. brGO/Mb bECs were placed in the culture medium with cells previously grown in six-well plates (Figure 6a). The packageless bEC was capable of utilizing ions in the cell culture medium for charging and discharging (Figure 6b,c). CVs at different scan rates showed nearly rectangular shapes up to 500 mV s^{-1} indicating almost ideal capacitive behavior (Figure 6d). The toxicity of the brGO/Mb bEC was tested by charging and discharging the packageless device in a MEF and COS-7 cell medium for 5000 cycles at high current density for 3 h. No change in cell morphology or dead/live cell ratio was found due to the cycling test, indicating no toxic effects on live cells on short term as measured by the trypan blue assay (Figure 6e,f; and Figure S23, Supporting Information). The cell viability after the charge–discharge regimen was found to be identical and no significant differences with respect to the control cell population ($p < 0.01$, paired student's t-test).

The brGO/Mb in a packageless platform makes the bEC devices ultrathin, light weight, and completely flexible. However, before using the packageless platform of the bEC device in any long-term implantable applications, the stability of the device components has to be evaluated for long-term use. The long-term stability of the brGO/Mb electrode was evaluated using QCM after the film was exposed to 96 h of continuous charge and discharge cycles in water (50×10^{-3} M NaCl was added to provide ions for the charge–discharge process) in open cell solution. Results show a small decrease in the mass of the film from 5.0 to 4.7 μg cm^{-2} which indicate a stable brGO/Mb electrode. However, the polyvinyl acetate (PVA) separator of the packageless sandwich device showed limited stability in open cell solution, and started to break and diffuse into the surrounding solution after only 27 h. Thus, PVA is not a suitable separator for the long-term cycling of the packageless bECs in open cell solution, and more research is needed to develop more stable separators for long-term use.

We then evaluated encapsulating the brGO/Mb device in polydimethylsiloxane (PDMS). The PDMS was chosen as a packaging material because of its low toxicity, flexibility, and light weight.[36] bECs showed the exact electrochemical behavior with and without PDMS packaging while maintaining complete flexibility (Figure 7d). Moreover, the PVA separator remained intact throughout the long-term cycling of the PDMS-packaged bECs for four continuous days (90,192 cycles) while the bEC was immersed in COS-7 cell culture medium. Cycling for 4 d provided enough time for the cells to make two full cycles of cell division. During the entire charging–discharging process, the growing cells were monitored by optical microscopy and no perceptible difference in the cell multiplication and overall morphology was found between control and bEC test cells (Figure 6g,h). No perceptible difference in the overall IDH metabolic activity was found between control cells and the cells subjected to continuous charging and discharging for 96 h. Results clearly show that PDMS device packaging is very efficient in maintaining the integrity of performance with no toxic effects on cells. In addition, the drop in the areal capacitance after cycling the device for 96 h was only 11%. These results suggest that brGO/Mb devices could work efficiently as implantable power sources in packageless platform for short term and for long term in PDMS-encapsulated design with good stability.

Since implantable bioelectronics are always subject to movement inside the patient's body, brGO/Mb bEC performance was evaluated at different bending conditions (Figure 7). The ultrathin brGO/Mb bEC showed excellent tolerance for bending to different angles (Figure 7a) with no change in capacitance even after bending to 180°. However, a slight decrease in capacitance was observed when the device was subjected to 1000 charge/discharge cycles while bent at 90° (Figure 7b). In addition, the brGO/Mb device showed no loss of performance after bending to 1000 bending cycles to an angle of 90° (Figure 7c). These results suggest that the brGO/Mb bECs are robust under bending stresses in both packaged and packageless designs which make these bEC suitable for the different bending conditions expected for implantable bioelectronics.

Electrochemical impedance spectroscopy showed nearly straight lines in the high-frequency region in all tested electrolytes (Figure S24a, Supporting Information). The brGO/Mb device showed multiple time constants behavior with cell time constant of only 1.5 ms in biofluids at a frequency of −45° (Figure S24b, Supporting Information). In addition, the downturn of the phase angle at low frequency (<1 Hz) is mainly due to the leakage current/voltage from the packageless devices (Figure S25, Supporting Information). Three packageless bECs made up of the ultrathin brGO/Mb films were yet capable of efficiently powering a light emitting diode utilizing calf serum as the electrolyte (Figure S24, Supporting Information). On the other hand, the rapid performance of our devices is likely to be related to fast ion movement through our thin electrode assemblies with myoglobin possibly acting as a nanochannel for fast ion transport.[37]

In summary, novel brGO-protein bECs were fabricated with high volumetric capacitances up to 655 F cm^{-3} in bio-fluids. Proteins bound to GO sheets played multiple roles in fabricating safe and high-performance bECs. First, proteins rendered the GO sheets nontoxic to cell-containing environments even at high concentrations. Moreover, proteins provide pseudocapacitive behavior for charge/discharge through their heteroatom-rich nanostructures

and the high abundance of the protonatable charged amino acid residues. Finally, protein layers provide nanopores that may act as nanochannels for shuttling ions in the biofluids to the conductive graphene interlayers. These new devices retained high energy density comparable to that of Li thin film batteries while utilizing serum/urine or cell media as electrolytes to power LEDs with little loss of performance, and no cell toxicity after 5000 cycles in pack-ageless platform and ≈90 K cycles in PDMS-packaged design. Unlike batteries that suffer from relatively slow discharge rates, the ultrathin brGO/Mb bECs have much faster performance making these devices perfect for the fast discharge of electrical signals to the implanted biomedical devices. With protein as a major component and utilizing body fluids for electrolyte function, these devices have the potential to power the next-generation miniaturized bioelectronics.

3. Experimental Section

Electrode Fabrication

Fabrication of brGO/Mb electrodes starts by reacting the surface of the thin gold current collector with 5×10^{-3} M mercaptopropionic acid in 70% ethanol to self-assemble an anionic alkylthiol monolayer. Next, PDDA was adsorbed from a 4.0 mg mL^{-1} solution in 0.5 M NaCl onto the gold surface to form a cationic hydrophilic/hydrophobic underlayer suitable for adsorbing the next layers. A negatively charged layer was then adsorbed from 0.7 mg mL^{-1} bGO in pH 7.2 buffer, followed by a layer of cationic Mb adsorbed from 3.0 mg mL^{-1} solution, pH 5.0. In this way, three layers of bGO were sandwiched between two layers of myoglobin, and named as a bGO/Mb film. Electrochemical reduction of the bGO/Mb film was then performed using amperometry at a constant potential of −1.2 V for 70 s in 10×10^{-3} M acetate buffer, pH 5.5 in 0.5 M salt such as KBr or lithium perchlorate ($LiClO_4$), and the resulting film named brGO/Mb.

Device fabrication and testing

A thin water-insoluble PVA separator with an average thickness of 992 nm was sandwiched between two brGO/Mb electrodes in a bottom-up designed supercapacitor and wrapped with Kapton tape. PVA was first diluted in the test electrolyte solution to a concentration of 1–5%. Adjustments may be needed until achieving full intact thin layer. The diluted suspension of PVA was then applied to one side of the bEC, left to be just partially wet, and then the device was assembled. The full stack thickness of the device is 1.14 μm including electrodes, current collectors, and separators. The device was then dipped into the testing electrolyte for 10 min before electrochemical performance was evaluated to ensure the wetting of the electrodes with the test electrolyte. The device was connected to the electrochemical workstation through extension from the gold collector via alligator clips, while copper tape was used to connect the device to the electrochemical workstation when using cell culture media as electrolyte to avoid the possible contamination of the workstation alligator clips by the media. A midstream urine sample was collected from a healthy male individual and used as an electrolyte. Informed signed consent was obtained from the sample donor.

Supplementary Material

Refer to Web version on PubMed Central for supplementary material.

Acknowledgments

The authors are grateful for financial support from U.S. PHS grants EB016707 and EB014586 from the National Institute of Biomedical Imaging and Bioengineering NIH, ES03154 (J.F.R.) and ES023350 (A.K.B.) from the National Institute of Environmental Health Sciences (NIEHS), NIH, and NSF EAGER grant (DMR-1441879) (C.V.K.). The authors thank Abdelhamid El-sawy, MD Shakil, Lhacene Adnane, and Raihan Khan for helping with SEM imaging and conductivity measurements. The authors thank Flavio Maran and Steven Suib for valuable discussions.

References

1. Hannan MA, Mutashar S, Samad SA, Hussain A. Biomed Eng Online. 2014; 13:79. [PubMed: 24950601]
2. a) Karami, M Amin, Inman, DJ. Appl Phys Lett. 2012; 100:042901.b) Starner T. IBM Syst J. 1996; 35:618.
3. a) Falk M, Villarrubia CWN, Babanova S, Atanassov P, Shleev S. ChemPhysChem. 2013; 14:2045. [PubMed: 23460490] b) Kerzenmacher S, Ducrée J, Zengerle R, von Stetten F. J Power Sources. 2008; 182:1.c) Yuan R, Kelly MM, David PA. J Phys: Conf Ser. 2013; 476:012011.
4. Wang ZL. Sci Am. 2008; 298:82.
5. Zheng Q, Shi B, Fan F, Wang X, Yan L, Yuan W, Wang S, Liu H, Li Z, Wang ZL. Adv Mater. 2014; 26:5851. [PubMed: 25043590]
6. Zurbuchen A, Pfenniger A, Stahel A, Stoeck CT, Vandenberghe S, Koch VM, Vogel R. Ann Biomed Eng. 2013; 41:131. [PubMed: 22805983]
7. a) Wang ZL, Wu W. Angew Chem, Int Ed Engl. 2012; 51:11700. [PubMed: 23124936] b) Yuan L, Xiao X, Ding T, Zhong J, Zhang X, Shen Y, Hu B, Huang Y, Zhou J, Wang ZL. Angew Chem, Int Ed Engl. 2012; 51:4934. [PubMed: 22473807]
8. a) Xiao X, Li T, Yang P, Gao Y, Jin H, Ni W, Zhan W, Zhang X, Cao Y, Zhong J, Gong L, Yen WC, Mai W, Chen J, Huo K, Chueh YL, Wang ZL, Zhou J. ACS Nano. 2012; 6:9200. [PubMed: 22978389] b) Yin L, Huang X, Xu H, Zhang Y, Lam J, Cheng J, Rogers JA. Adv Mater. 2014; 26:3879. [PubMed: 24652717]
9. a) Simon P, Gogotsi Y. Nat Mater. 2008; 7:845. [PubMed: 18956000] b) Kim SK, Kim HJ, Lee JC, Braun PV, Park HS. ACS Nano. 2015; 9:8569. [PubMed: 26192922]
10. a) Hanker JS, Giammara BL. Science. 1988; 242:885. [PubMed: 3055300] b) Venkatraghavan L, Chinnapa V, Peng P, Brull R. Can J Anaesth. 2009; 56:320. [PubMed: 19296193]
11. a) Burke A. Electrochim Acta. 2007; 53:1083.b) Simon P, Gogotsi Y. Acc Chem Res. 2013; 46:1094. [PubMed: 22670843]
12. Armand M, Tarascon JM. Nature. 2008; 451:652. [PubMed: 18256660]
13. Xue Y, Ding Y, Niu J, Xia Z, Roy A, Chen H, Qu J, Wang ZL, Dai L. Sci Adv. 2015; 1:e1400198. [PubMed: 26601246]
14. a) Kadimisetty K, Mosa IM, Malla S, Satterwhite-Warden JE, Kuhns TM, Faria RC, Lee NH, Rusling JF. Biosens Bioelectron. 2016; 77:188. [PubMed: 26406460] b) El-Kady MF, Shao Y, Kaner RB. Nat Rev Mater. 2016; 1:16033.
15. a) El-Kady MF, Strong V, Dubin S, Kaner RB. Science. 2012; 335:1326. [PubMed: 22422977] b) Yoo JJ, Balakrishnan K, Huang J, Meunier V, Sumpter BG, Srivastava A, Conway M, Reddy AL, Yu J, Vajtai R, Ajayan PM. Nano Lett. 2011; 11:1423. [PubMed: 21381713]
16. a) Liao KH, Lin YS, Macosko CW, Haynes CL. ACS Appl Mater Interfaces. 2011; 3:2607. [PubMed: 21650218] b) Schinwald A, Murphy FA, Jones A, MacNee W, Donaldson K. ACS Nano. 2012; 6:736. [PubMed: 22195731]
17. Pattammattel A, Puglia M, Chakraborty S, Deshapriya IK, Dutta PK, Kumar CV. Langmuir. 2013; 29:15643. [PubMed: 24274382]

18. Rusling, JF. Biomolecular films: design, function, and applications. Taylor and Francis; New York: 2003.
19. a) Ferrero GA, Fuertes AB, Sevilla M. Sci Rep. 2015; 5:16618. [PubMed: 26568473] b) Wu Z-S, Parvez K, Winter A, Vieker H, Liu X, Han S, Turchanin A, Feng X, Müllen K. Adv Mater. 2014; 26:4552. [PubMed: 24782095]
20. Shukla R, Bansal V, Chaudhary M, Basu A, Bhonde RR, Sastry M. Langmuir. 2005; 21:10644. [PubMed: 16262332]
21. Gu Z, McDermott A. J Am Chem Soc. 1993; 115:4282.
22. Gan S, Zhong L, Gao L, Han D, Niu L. J Am Chem Soc. 2016; 138:1490. [PubMed: 26797173]
23. Tung VC, Allen MJ, Yang Y, Kaner RB. Nat Nanotechnol. 2009; 4:25. [PubMed: 19119278]
24. Moon IK, Lee J, Ruoff RS, Lee H. Nat Commun. 2010; 1:73. [PubMed: 20865806]
25. Xue T, Jiang S, Qu Y, Su Q, Cheng R, Dubin S, Chiu CY, Kaner R, Huang Y, Duan X. Angew Chem, Int Ed. 2012; 51:3822.
26. Khairy M, El-Safty SA. Chem Commun. 2014; 50:1356.
27. Majorek KA, Porebski PJ, Dayal A, Zimmerman MD, Jablonska K, Stewart AJ, Chruszcz M, Minor W. Mol Immunol. 2012; 52:174. [PubMed: 22677715]
28. Angnes L, Richter EM, Augelli MA, Kume GH. Anal Chem. 2000; 72:5503. [PubMed: 11080906]
29. Simon P, Gogotsi Y, Dunn B. Science. 2014; 343:1210. [PubMed: 24626920]
30. Lee SW, Kim J, Chen S, Hammond PT, Shao-Horn Y. ACS Nano. 2010; 4:3889. [PubMed: 20552996]
31. Yun YS, Cho SY, Shim J, Kim BH, Chang SJ, Baek SJ, Huh YS, Tak Y, Park YW, Park S, Jin HJ. Adv Mater. 2013; 25:1993. [PubMed: 23436254]
32. Malvankar NS, Mester T, Tuominen MT, Lovley DR. ChemPhysChem. 2012; 13:463. [PubMed: 22253215]
33. Hur J, Im K, Hwang S, Choi B, Kim S, Hwang S, Park N, Kim K. Sci Rep. 2013; 3:1282. [PubMed: 23412432]
34. Kotani E, Yamamoto N, Kobayashi I, Uchino K, Muto S, Ijiri H, Shimabukuro J, Tamura T, Sezutsu H, Mori H. Sci Rep. 2015; 5:11051. [PubMed: 26053044]
35. Jastrzębska AM, Kurtycz P, Olszyna AR. J Nanopart Res. 2012; 14:1320. [PubMed: 23239936]
36. Kim SH, Moon JH, Kim JH, Jeong SM, Lee SH. Biomed Eng Lett. 2011; 1:199.
37. a) Jiang Y, Kirmizialtin S, Sanchez IC. Sci Rep. 2014; 4:4011. [PubMed: 24500195] b) Levantino M, Schiro G, Lemke HT, Cottone G, Glownia JM, Zhu D, Chollet M, Ihee H, Cupane A, Cammarata M. Nat Commun. 2015; 6:6772. [PubMed: 25832715]

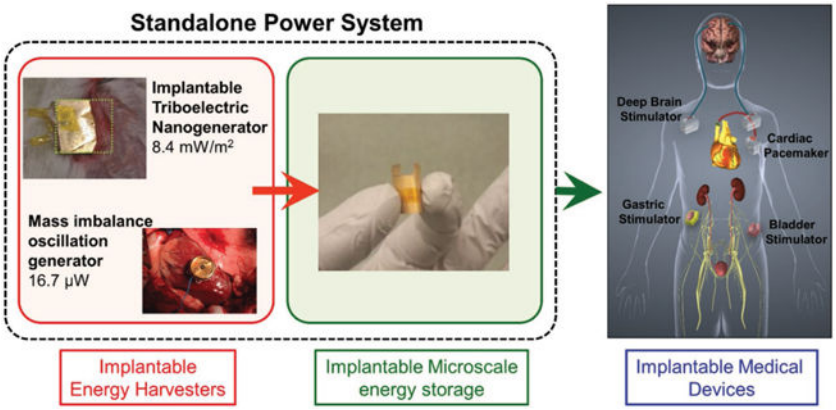

Figure 1.

Scheme illustrating our vision for the brGO/Mb bECs (center panel) as micropower sources for biomedical implants. Energy harvesters in the left panel were reproduced with permission.[5,6] Copyright 2014, John Wiley and Sons and Copyright 2013, Springer, respectively.

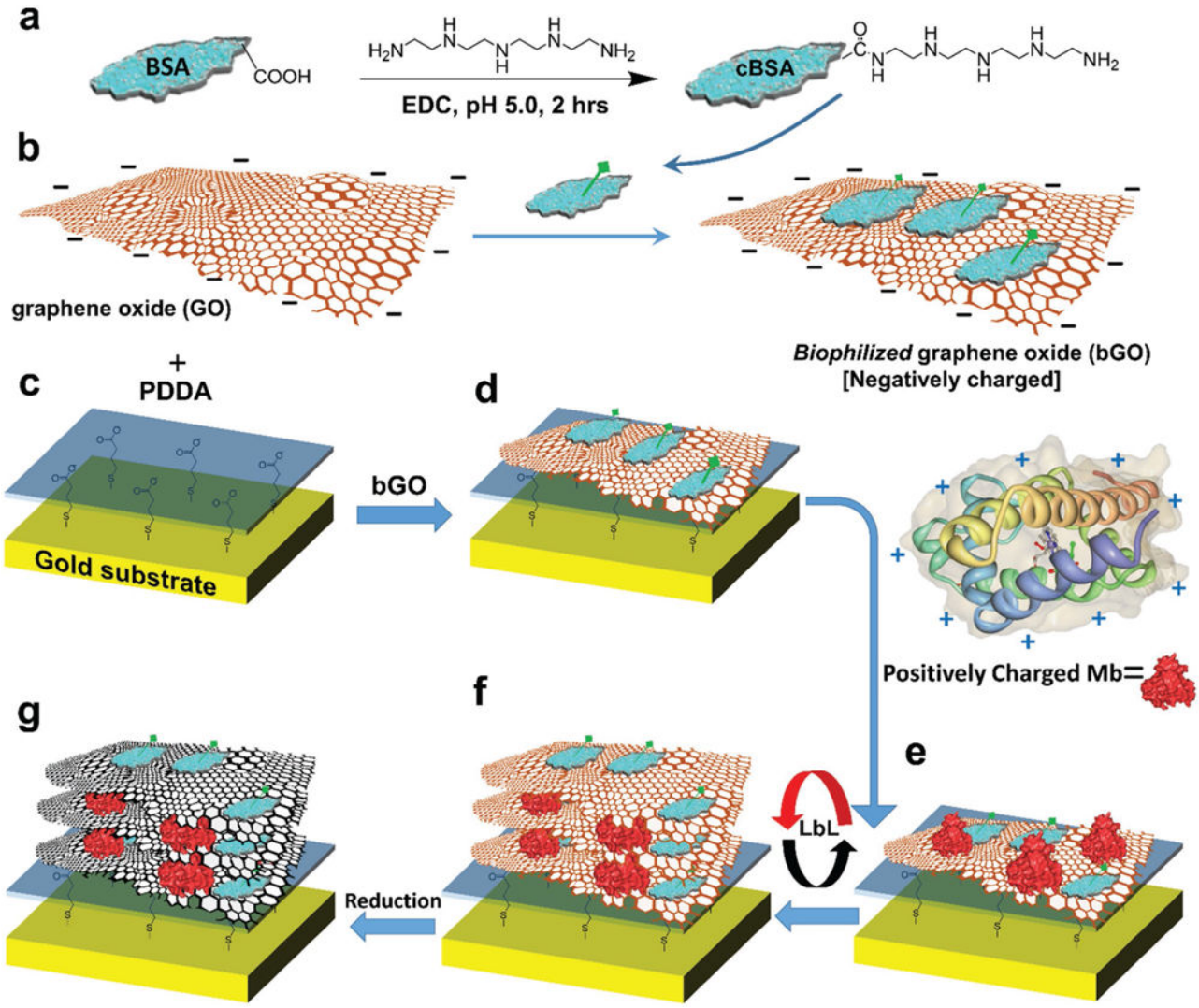

Figure 2.

Illustration of the electrode fabrication. a) Preparation of cationized bovine serum albumin (cBSA) by coupling the COOH groups of BSA with tetraethylenepentamine. b) Adsorbing cBSA onto GO sheets. c) Gold current collector with monolayer of mercaptopropionic acid, and a layer of polycation polydiallyldimethylammonium chloride (PDDA) adsorbed on top. d) Adsorption of bGO, e) adsorption of Mb, and f) film from LbL assembly of three bGO layers alternated with two Mb layers (abbreviated as bGO/Mb). g) Electrochemically reduced film (abbreviated as brGO/Mb).

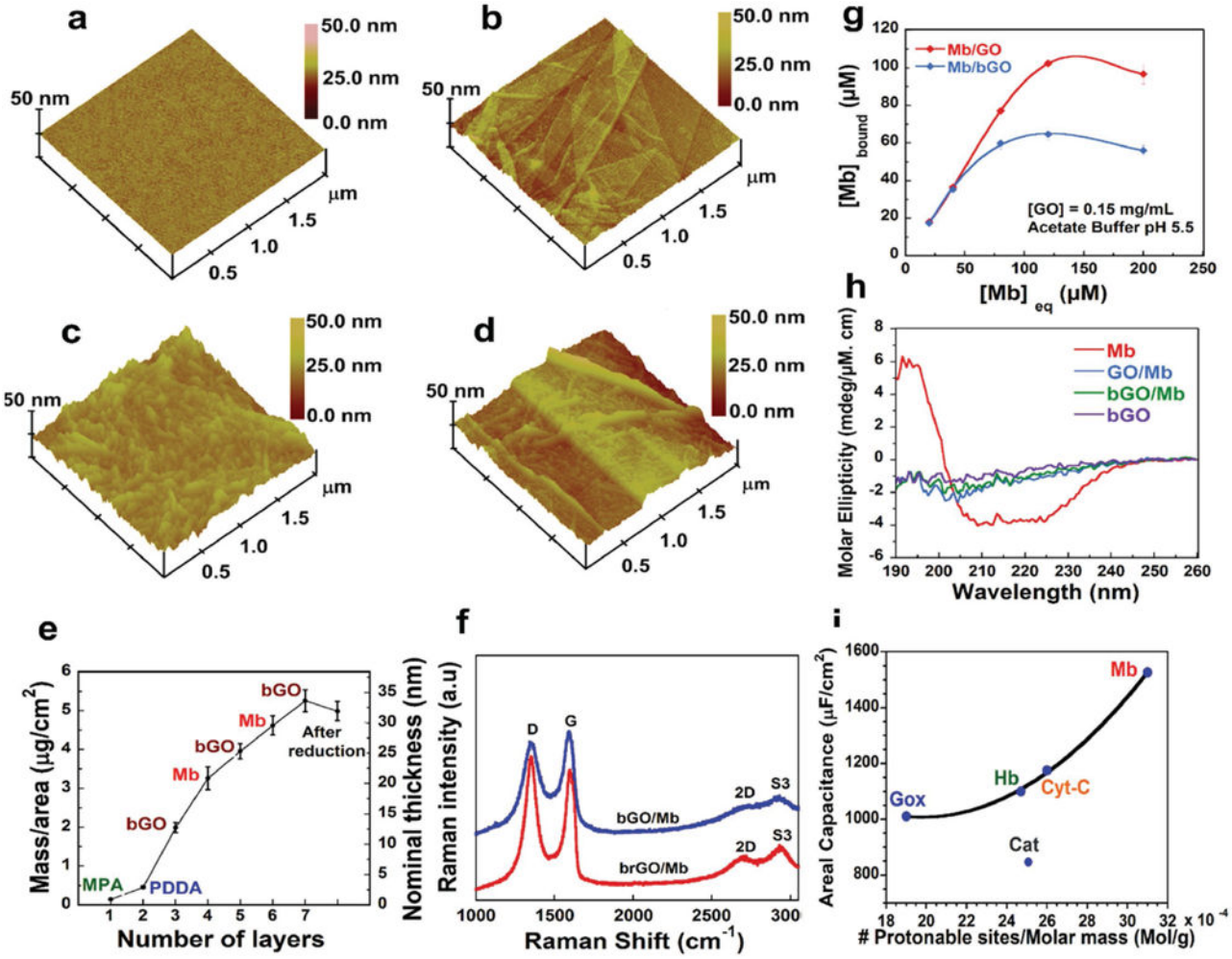

Figure 3.

Characterization of the graphene–protein hybrid electrodes. a–d) Tapping mode AFM images of the layer-by-layer assembled film on a mica disc. a) PDDA, b) PDDA-bGO, c) PDDA-bGO-Mb, and d) PDDA-bGO-Mb-bGO. e) Change in the mass/area and nominal thickness of the film as a function of the number of layers assembled as measured by quartz crystal microbalance (QCM). f) Raman spectra of films before and after electrochemical reduction. g) Myoglobin binding to GO (red curve) and bGO (blue curve) in 10×10^{-3} M acetate buffer at pH 5.5 as a function of increasing concentrations of myoglobin. h) Circular dichroism spectra suggesting extensive denaturation of Mb upon binding to either GO or bGO. i) Areal capacitance of three bilayers of brGO/protein in correlation to the number of sites available for protonation/deprotonation normalized by the molar mass of proteins. Cyt-C, Mb, Hb, GOx, and Cat stand for cytochrome-C, myoglobin, hemoglobin, glucose oxidase, and catalase, respectively. The highest areal capacitance among these proteins was observed with brGO/Mb film.

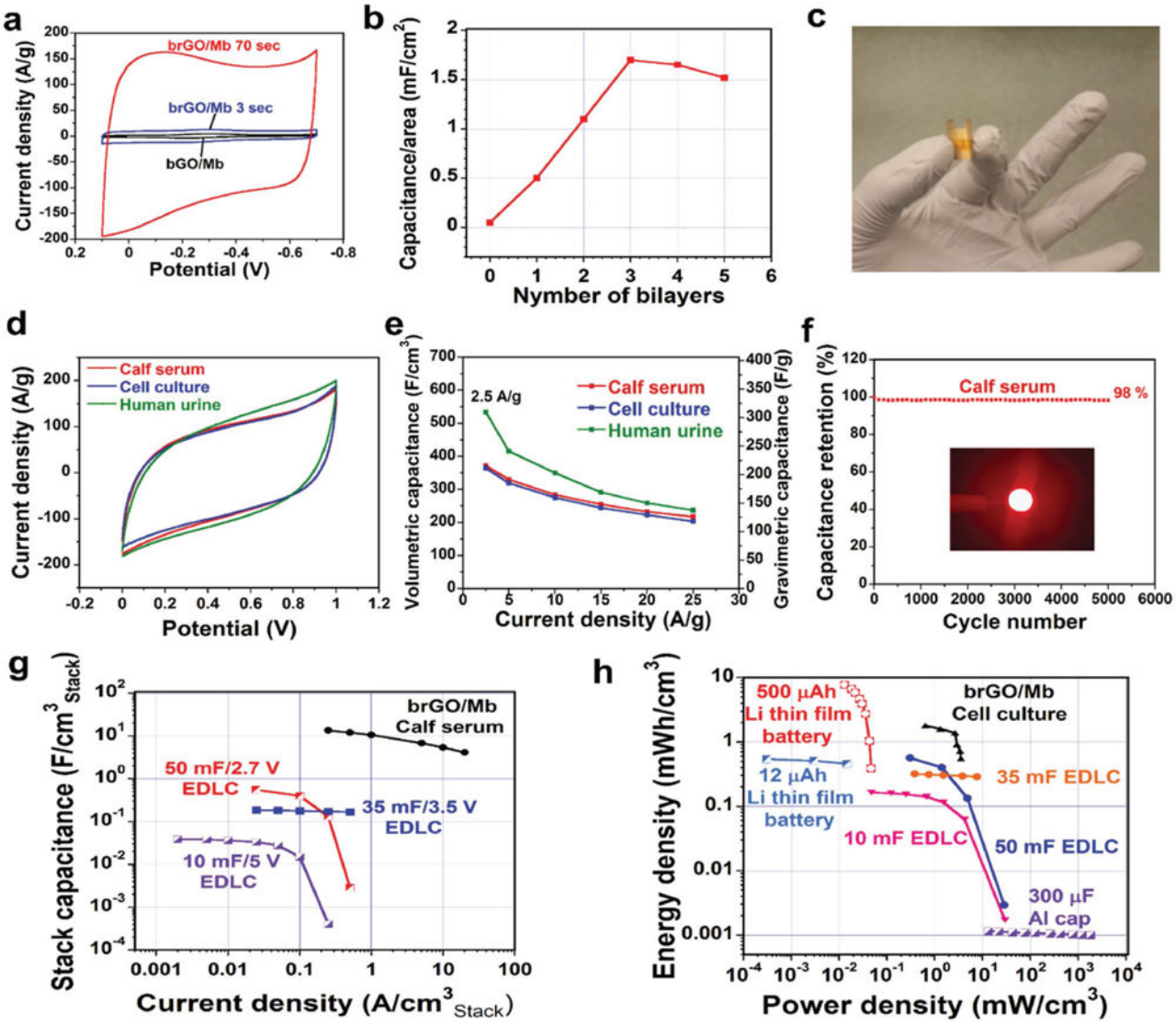

Figure 4.

Electrochemical behavior of a brGO/Mb bEC. a) Cyclic voltammetry (CV) at 300 mV s^{-1} of nonreduced film (bGO/Mb), and electrochemically reduced film (brGO/Mb) for 3 and 70 s. b) Optimization of the film capacitance with the number of bilayers showing the highest capacitance for three bilayers. c) Photograph of the packageless brGO/Mb EC. d) Cyclic voltammetry at 1000 mV s^{-1} of brGO/Mb film in different electrolytes. e) Change of volumetric and gravimetric capacitance with moderate-to-high current density for a brGO/Mb electrode in biofluids. f) Cyclic stability of the brGO/Mb bEC in calf serum, inset shows LED powered by three brGO/Mb bECs connected in series with calf serum saturated separators. g) Volumetric stack capacitance of a brGO/Mb bEC at different current densities as compared to commercial electrical double layer capacitors (EDLC). h) Energy and power densities of a brGO/Mb bEC in a cell culture medium as compared to commercial EDLC, 300 µF/3 V aluminum electrolytic capacitor, 12 µA h/3.3 V Li thin film battery, and 500 µA h/5 V Li thin film battery.

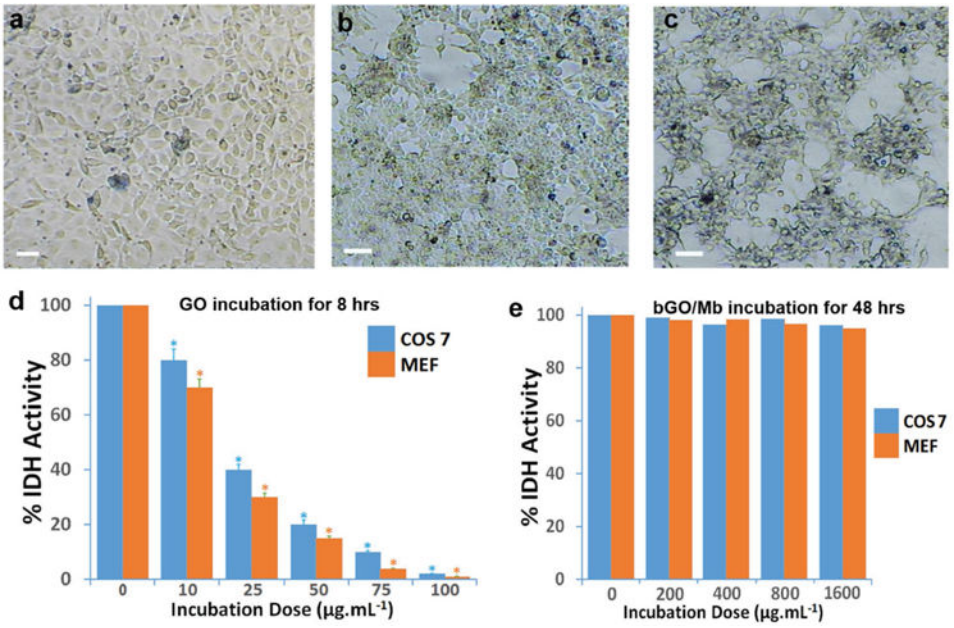

Figure 5.

Toxicity of bGO/Mb versus the as-prepared GO. a–c) Optical microscopy images of COS-7 cells, scale bar is 10 μm. a) Healthy control COS-7 cells without addition of any graphene-based materials. b) COS-7 cells coincubated for 48 h with 1600 μg mL^{-1} protein modified graphene oxide (bGO/Mb) showing no adverse effects on cells compared to control. c) COS-7 cells coincubated for only 8 h with 25 μg mL^{-1} of the as-prepared GO showing severe cell damage. d) Dose-dependent toxicity in COS-7 and MEF cells coincubated with GO for 8 h, measured in terms of the intracellular dehydrogenases (IDH) activity. e) No significant cell toxicity was observed in COS-7 and MEF cells coincubated with bGO/Mb as measured by IDH activity even at very high concentrations.

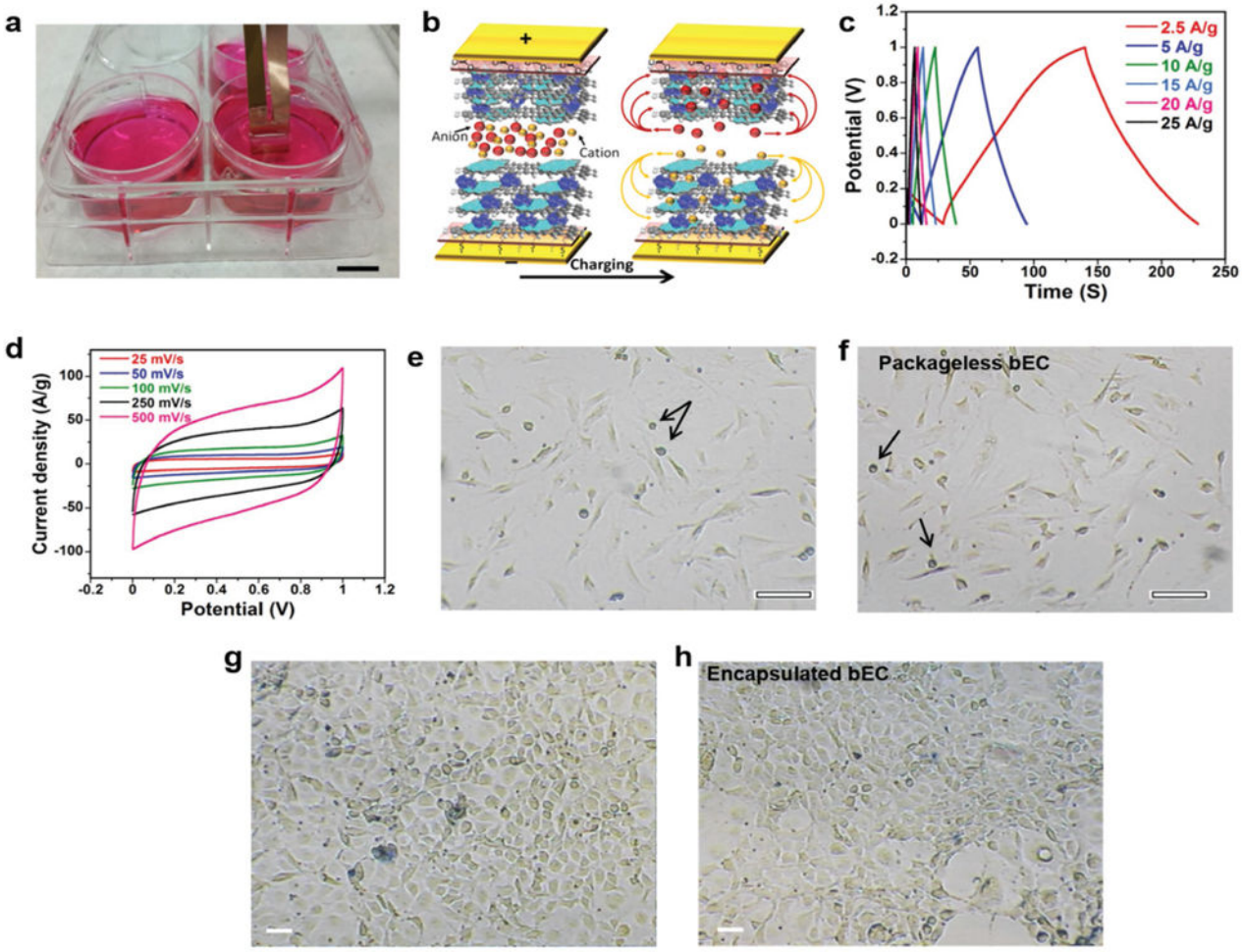

Figure 6.

Performance of brGO/Mb supercapacitor in cell culture medium. a) Photograph of plastic supported bEC device dipped in six-well plate containing MEF cells in DMEM, and connected to the electrochemical workstation via copper tape. The scale bar is 1.0 cm. b) Scheme showing movement of the ions available in cell culture medium during charging process. c) Charge/discharge cycles at different current densities in the cell media. d) CV curves at different scan rates in cell media. e,f) Optical microscopy images for MEF cells stained with trypan blue subjected to zero and 5000 charge/discharge cycles, respectively, of the packageless bEC for 3 h. Both (e) and (f) show live cells appeared with a very small number of dead cells (stained blue-green, black arrows show examples). The absence of differences suggests insignificant cell death due to brGO/Mb bEC operation in the cell culture (scale bar is 50 μm). g,h) Optical microscopy images for COS-7 cells stained with trypan blue. g) Control cells with zero charge/discharge cycles. h) Cells subjected to long-term cycling test of the polydimethylsiloxane (PDMS)-packaged bEC for 96 h (≈90 K cycles), showing no difference in cell death as compared to control cells.

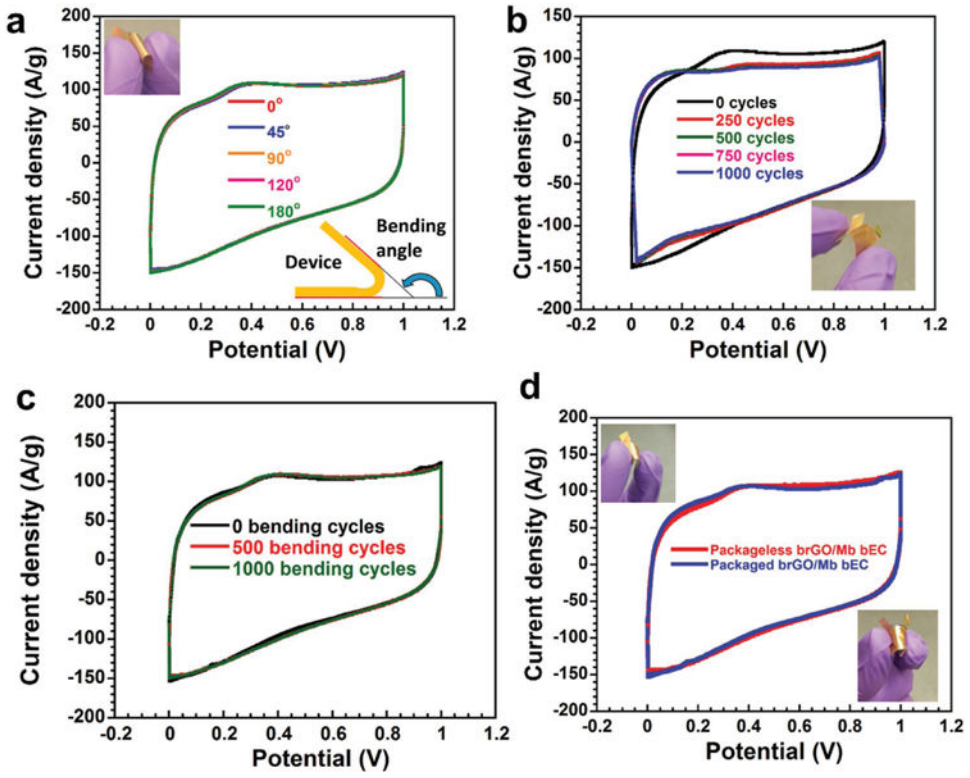

Figure 7.

CVs of brGO/Mb bEC showing a) the effect of bending the device to different angles, b) the effect of charging/discharging the device to different number of cycles while the device is bent to an angle of 90°, and c) the effect of manually bending the brGO/Mb device to different bending cycles. The device was bent to an angle of 90° in each cycle. d) The electrochemical performance of the brGO/Mb bEC in packageless and PDMS-packaged platforms bent to a 90° angle.